
ADMN: A Layer-Wise Adaptive Multimodal Network for Dynamic Input Noise and Compute Resources

Jason Wu¹ Kang Yang¹ Lance Kaplan² Mani Srivastava^{1,3,4}

Abstract

Multimodal deep learning systems are deployed in dynamic scenarios due to the robustness afforded by multiple sensing modalities. Nevertheless, they struggle with varying compute resource availability (due to multi-tenancy, device heterogeneity, etc.) and fluctuating quality of inputs (from sensor feed corruption, environmental noise, etc.). Current multimodal systems employ static resource provisioning and cannot easily adapt when compute resources change over time. Additionally, their reliance on processing sensor data with fixed feature extractors is ill-equipped to handle variations in modality quality. Consequently, uninformative modalities, such as those with high noise, needlessly consume resources better allocated towards other modalities. We propose ADMN, a layer-wise Adaptive Depth Multimodal Network capable of tackling both challenges - it adjusts the total number of active layers across all modalities to meet compute resource constraints, and continually reallocates layers across input modalities according to their modality quality. Our evaluations showcase ADMN can match the accuracy of state-of-the-art networks while reducing up to 75% of their floating-point operations.

1. Introduction

Background: Multimodal deep learning systems fusing sensory data from various modalities are the standard for accurate, robust sensing (Chen et al., 2022; Eitel et al., 2015). The robustness of multimodality arises from *redundant information* captured across modalities, which mitigates the effect of sensor failure, noise corruption, and adverse environmental conditions (Lin & Hu, 2023; Liu et al., 2022). Accordingly, these multimodal systems are invaluable in

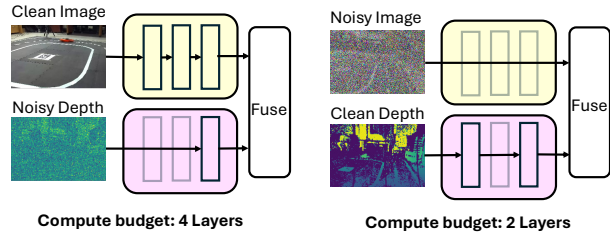


Figure 1. Overview of ADMN. Variable depth backbones adapt to both changing compute resources and input noise characteristics

highly dynamic environments, where a given input modality’s quality-of-information (QoI) can vary drastically across samples. QoI refers to the information content of the sensor data, where noise-corrupted modalities would be classified as low-QoI. Fluctuations in a modality’s QoI can occur over long periods of time (e.g., lighting conditions over the day), or rapidly (e.g., battlefield settings or unstable sensor feeds).

Challenges: Although multimodal robustness allows these deep learning systems to deal with highly variable QoI, the first challenge surrounds *efficiency of such systems*. State-of-the-art multimodal networks employ *static provisioning* in which inputs proceed through a fixed computational graph established by the architecture (Wang et al., 2024; Yin et al., 2024). Consequently, each modality’s data is fully processed by the network with no regard to variable input QoI, and valuable compute resources may be wasted on low-QoI modalities. In particular, systems with considerable energy or latency constraints will suffer greatly from this misallocation. *We hypothesize that flexibly allocating computational resources among modalities in accordance to each modality’s QoI on a per-sample basis can greatly boost model performance in compute-limited settings.*

In addition to its inability to adapt to the varying QoI of the input modalities, static provisioning also struggles with the second challenge of *dynamic compute resources*. The highly dynamic, real-world environments in which multimodal systems are particularly relevant tend to also suffer from variable computing resource availability over time. For instance, the deployment platforms can be affected by thermal throttling, energy fluctuations, or multi-tenancy. Unfortunately, statically provisioned models are unable to adjust their resource usage to meet dynamic compute re-

¹University of California, Los Angeles ²US Army DEVCOM Army Research Laboratory ³Amazon ⁴Mani Srivastava holds concurrent appointments as an Amazon Scholar and a Professor at UCLA, but the work in this paper is unrelated to Amazon. Correspondence to: Jason Wu <jaysunwu@g.ucla.edu>.

source constraints. A naive solution uses *model selection* in which several models of different sizes are trained and deployed for various levels of compute resource availability. Aside from the obvious drawback of requiring an unreasonable amount of training resources, it also complicates the standard practice of initializing multimodal networks with pretrained weights prior to finetuning (Manzoor et al., 2023). Publicly available pretrained weights only exist for a few configurations of model size, with fewer options for uncommon sensing modalities. *We hypothesize that a single network, initialized with pretrained weights, which can dynamically adjust its resource usage, offers an effective solution to the challenge of fluctuating compute resources.*

Proposed Solution: We propose ADMN, an Adaptive Depth Multimodal Network jointly tackling the challenges of adaptation to both dynamic compute resources and variable QoI inputs. While these challenges are agnostic to the multimodal fusion method (e.g., data-level (Kim et al., 2021), embedding-level (Jeong et al., 2024), and late (Samplawski et al., 2023)), we focus specifically on embedding-level fusion due to applicability and ease of implementation. Figure 1 provides a high-level depiction of ADMN. Following the standard for embedding-level fusion, each modality is processed with an independent backbone before undergoing fusion with a transformer encoder.

First, ADMN addresses the challenge of *dynamic compute resources* with adaptive backbones containing adjustable layer configurations. With the same set of model weights, ADMN activates a subset of backbone layers according to the available compute resources. We accomplish this by training large backbones initialized with pretrained weights while stochastically dropping layers in every modality’s backbone through the LayerDrop technique (Fan et al., 2019). We extend the unimodal, text-only LayerDrop technique to not only Vision Transformers, but also multimodal networks. Such a strategy produces a novel multimodal network whose backbones are resilient to missing layers at test-time, allowing for the usage of fewer layers during resource scarcity.

Second, given a total layer budget established by the available resources, ADMN addresses the challenge of *dynamic QoI* by adapting the choice of selected backbone layers according to each modality’s QoI. Our approach trains a multimodal controller on top of the adaptive backbones. The controller learns an optimal layer allocation among the backbones, conditioned on the relative QoI across the modalities of a given input sample. We propose a simple training procedure leveraging Gumbel-Softmax Sampling (Maddison et al., 2016) and the straight-through estimator (Bengio et al., 2013) to enable end-to-end training without costly reinforcement learning.

We benchmark ADMN against several baselines to demonstrate its ability to preserve accuracy while simultaneously

minimizing energy and latency costs. ADMN is tested on both multimodal localization and multimodal action recognition tasks, reinforcing its generality and applicability. ADMN can match the performance of larger state-of-the-art models while reducing FLOPS by up to 75% and latency by up to 60%. We release our code at <https://anonymous.4open.science/r/ADMN-15C9/>. Our contributions are summarized as below:

- We present an adaptive multimodal network where resource allocation among modality backbones is dictated by QoI characteristics and current computational resource availability at inference time for every sample.
- We adapt the LayerDrop technique from its original domain of text transformers to multimodal visual networks by introducing *full-modality dropout*, and demonstrate that this technique can be generalized to diverse tasks such as localization and classification.
- We design a multimodal controller that can be trained from end-to-end with a simple method to propagate gradients to the controller.
- Experiments on multimodal localization and human activity recognition tasks across different modalities demonstrate ADMN’s efficiency.

2. Related Work

Early Exiting in Unimodal Networks. Early Exiting has been explored extensively in unimodal networks to improve inference efficiency (Xin et al., 2020; Zhou et al., 2020; Meng et al., 2022). Methods like DeeBERT (Xin et al., 2020) and PABEE (Zhou et al., 2020) use confidence thresholds to halt computation for simpler inputs. However, these unimodal approaches fail to consider multimodal challenges such as QoI-aware resource allocation. Moreover, Early Exiting is incompatible with redistributing resources away from low-QoI modalities, as these low-confidence samples propagate through the entire network.

Dynamic Inference for Multimodal Systems. Multimodal networks traditionally rely on input-agnostic static provisioning, resulting in inefficiencies when modality QoI varies, and also incompatibility with dynamic computational resource availability. To enhance computational efficiency, dynamic networks have been proposed (Xue & Marculescu, 2023; Panda et al., 2021; Gao et al., 2020; Cai et al., 2024; Mullapudi et al., 2018). DynMM (Xue & Marculescu, 2023) trains a set of expert networks representing different modality combinations, processing simple inputs with a subset of available modalities. AdaMML (Panda et al., 2021) and Listen to Look (Gao et al., 2020) improve inference efficiency by leveraging multimodal information to eliminate temporal redundancy in videos. ACF (Cai et al., 2024)

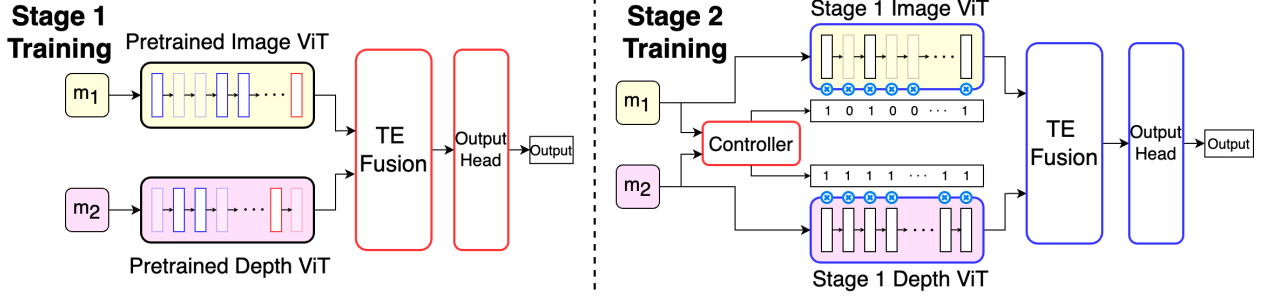


Figure 2. ADMN architecture. [Gray box]: dropped layer, [Blue box]: frozen layer, [Red box]: tunable layer. TE: Transformer Encoder.

dynamically replaces certain modules with lightweight networks according to the input for greater efficiency in edge devices. Despite these advances, these existing methods (1) overlook significant QoI variations arising from input noise, (2) utilize or discard entire modalities without fine-grained control, and (3) fail to consider *fixed* resource budgets. In contrast, ADMN allocates a fixed number of layers among modalities in a fine-grained manner according to input QoI, which accounts for both relative modality importance and noise.

3. Methodology

3.1. Problem Description

A typical multimodal system employing embedding-level fusion is illustrated on the left side of Figure 2. It first utilizes independent, modality-specific backbones to extract informative embeddings for each modality. These embeddings are fused via self-attention in a *Transformer encoder*, which condenses all modality embeddings into a single joint embedding. Finally, an output head converts the dense joint embedding into the desired final output specific to the target task. In this work, ADMN accomplishes two objectives. First, it contains dynamic backbones robust to various dropped layers, thus enabling adaptation to different total layer budgets. Second, it allocates the layer budget optimally among modality backbones (i.e., transformer layers) according to the fluctuating input QoI, greatly outperforming static models with the same layer budget.

3.2. ADMN Architecture

Figure 2 showcases the task-agnostic architecture of ADMN, which involves a two-stage training process.

Stage 1: LayerDrop Finetuning. We initialize each backbone with a set of weights pretrained with LayerDrop (Fan et al., 2019). Subsequently, the multimodal network is finetuned with LayerDrop on the desired task while freezing the majority of earlier backbone layers (shown in blue) to prevent overfitting. Stage 1’s objective is to adjust the learnable weights for the specific target task, while also training

the Fusion and Output layers to accept diverse embeddings arising from various backbone layer configurations.

Stage 2: Controller Training. We freeze all the Stage 1 network weights and train a controller that learns to allocate a fixed budget of L layers. The controller network accepts the multimodal inputs, and from the relative QoI, outputs a discrete sequence summing to L outlining the selection of backbone layers. Based on the task loss, the controller will readjust the layer allocation across the modalities.

3.3. Stage 1: LayerDrop Finetuning

We adapt the LayerDrop (Fan et al., 2019) work, originally designed for text input, to support non-text multimodal input, while also showcasing how LayerDrop can be integrated into modality pretraining.

3.3.1. VANILLA LAYERDROP

LayerDrop trained text transformers with layer-wise dropout, enabling on-demand depth reduction during test-time. During training, each layer of the transformer is dropped out with a certain probability, thereby forcing the network to function with only a subset of its layers. At inference time, they proposed a dropout strategy alternating layers starting from the middle to meet a particular compute requirement, referred to as the “every-other” strategy. We refer readers to the original work for greater detail.

3.3.2. MULTIMODAL LAYERDROP

We extend LayerDrop to Vision Transformers (ViTs) (Dosovitskiy, 2020) by first integrating them into ImageNet-1K (Russakovsky et al., 2015) pretraining. Rather than performing supervised training on ImageNet, which suffers heavily from convergence issues, we employ Masked Autoencoder (MAE) pretraining (He et al., 2022). We use a LayerDrop rate of 0.2 in each ViT layer and do not drop any layers in the decoder. By employing LayerDrop in MAE pretraining, the model learns to reason about the image in the presence of missing layers. Then, the MAE pretrained weights are loaded into each of the ViT backbones of a

multimodal (e.g., vision-depth) neural network to be finetuned on a downstream task. The majority of the backbone layers are frozen during finetuning, with the last few layers left tunable to adjust to the new task. A LayerDrop rate of 0.2 is maintained during the finetuning process in all the backbones, allowing the remaining learnable layers to adapt to the countless different combinations of missing layers. This process ultimately creates a task-specific multimodal network containing several ViT backbones with adaptable layer configurations at inference time.

Full-Backbone LayerDrop: One unique challenge that surfaces when applying LayerDrop in a multimodal context is the need to subject a backbone to extreme dropout conditions. In the unimodal case, dropping all layers of a backbone is avoided because it would leave the input unprocessed. For a multimodal network, however, one may wish to drop all layers of a modality that suffers from extreme noise. The typical LayerDrop training ratio of 0.2 in a 12 layer ViT is unlikely to drop out all layers of a given modality, resulting in unpredictable behavior when all layers are missing at test-time. Increasing the dropout rate is an option, but can hurt the full-layer performance. To remedy this, we employ full-backbone dropout during training time, under which there is a 10% chance all the layers of a given modality’s backbone will be dropped out independently of the 0.2 LayerDrop rate. Through this procedure, the fusion network can observe embeddings that emerge when one backbone’s layers are entirely bypassed, preventing them from potentially disrupting the self-attention process.

3.4. Stage 2: Controller Training

The controller decides which backbone layers to activate within the frozen Stage 1 network depending on the relative input modality QoI, as shown in Figure 2. For instance, in a multimodal image and depth network with a layer budget L , the controller may choose to allocate all L layers to the image backbone if it detects that depth is severely corrupted, and vice versa. The controller performs this adaptation on a *per-sample* basis. In order to maximize the resources provided to the main network, the controller should also remain as lightweight as possible.

3.4.1. CONTROLLER ARCHITECTURE

Figure 3 reveals the structure of the controller. First, we downsample the multimodal inputs to 100×100 and pass them through a series of modality specific lightweight convolutional networks. The goal of these convolutional networks is to produce embeddings containing information solely regarding each modality’s QoI, which can be accomplished from low-resolution data. With M input modalities, the convolutional networks produce M total noise embeddings, which are subsequently fused by a transformer encoder. The

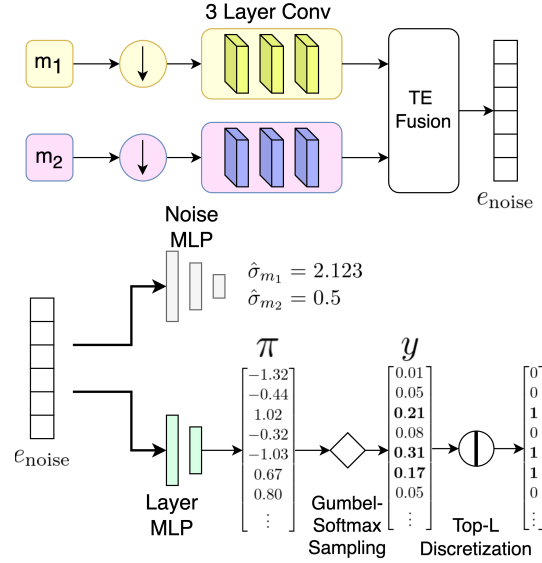


Figure 3. Detailed depiction of the ADMN controller. transformer encoder outputs a single embedding e_{noise} containing the noise signature of every input modality. From this joint noise embedding, we can obtain a set of raw logits

$$\pi = \text{MLP}(e_{\text{noise}}) \text{ where } \pi \in \mathbb{R}^C, C = \sum_{i=0}^M |b_i| \quad (1)$$

and $|b_i|$ is the number of layers in the backbone of modality m_i . In essence, π represents an allocation of L available layers among C total backbone layers, with values dependent on the noise characteristics of every input sample.

Ideally, the convolutional layers will automatically learn to extract each modality’s noise signature. Failure to identify the modality QoI will result in high loss arising from improper layer allocation, which will be backpropagated to the convolution. In practice, however, we found that adding supervision by providing ground truth noise information greatly aided convergence. Thus, we introduce an additional MLP that predicts the noise standard deviation $\hat{\sigma}_{m_i}$ of every modality m_i from e_{noise} . We optimize over the joint loss $\mathcal{L}_{\text{total}} = \mathcal{L}_{\text{model}} + \mathcal{L}_{\text{noise}}$, where $\mathcal{L}_{\text{noise}} = \sum_{i=0}^M |\hat{\sigma}_{m_i} - \sigma_{m_i}|$

3.4.2. DIFFERENTIABLE LAYER SELECTION

Although the logits π provide information regarding which layers to select, activating a given layer is a discrete, binary decision. One simple method is to perform *top-L masking* where the top- L largest logits are discretized to one and the rest are set to zero. The output of top- L masking is multiplied with the output of each backbone layer, zeroing out the contribution of dropped layers. While necessary for layer selection, the discretization process interrupts the flow of gradients during backpropagation. Consequently, the gradients from the frozen main network carrying vital

information on the success of a layer configuration will not propagate to the learnable parameters of the controller.

Traditional Unimodal Discretization: Gumbel-Softmax Sampling (Maddison et al., 2016) propagates gradients over discretization by approximating a categorical distribution while retaining differentiability, where

$$G = -\log(-\log(u)); u \sim U(0, 1) \quad (2)$$

defines the Gumbel distribution, and

$$y_i = \frac{\exp((\log(\pi_i) + g_i)/\tau)}{\sum_{j=1}^C \exp((\log(\pi_j) + g_j)/\tau)} \quad (3)$$

where y is the result of Gumbel-Softmax Sampling with i.i.d samples $g_{0...C} \sim G$. As the value of temperature τ decreases, y approximates a categorical distribution with a single $y_i = 1$ and the remaining $y_j = 0; j = 0...C, j \neq i$.

Unimodal Early-Exit methods rely upon Gumbel-Softmax Sampling (Meng et al., 2022). They employ decision networks at every layer of the model, outputting a single logit representing the likelihood of executing that particular layer, which then undergoes Gumbel-Softmax sampling.

Multimodal Discretization: Unfortunately, simply applying Gumbel-Softmax Sampling is insufficient for ADMN. The key difference between ADMN and unimodal Early-Exit works is that ADMN predicts the entire layer configuration at the *beginning of model execution, rather than forming a decision at every layer*. ADMN must decide the layer allocation by selecting L total layers based off characteristics from all modalities, and utilizing decision networks at every layer of the unimodal backbones would omit crucial multimodal information. Given this, emulating discretization solely through low-temperature Gumbel-Softmax sampling is a poor choice, as it approximates a categorical distribution in which *only a single layer is selected*.

We devise a method for retaining gradients over top- L sampling. Initially, we perform standard Gumbel-Softmax sampling with a temperature of 1 instead of a low temperature. This allows multiple high-value logits to be represented in the resulting probability distribution, better accommodating the selection of L layers. This is accomplished at the expense of the highly desirable near-discrete behavior of the low-temperature Gumbel-Softmax. We introduce a subsequent *top- L discretization* stage to activate only L layers, and maintain gradient flow through the *straight-through estimator* (Bengio et al., 2013). Represented by $y + (\text{discretize}(y) - y).\text{detach}()$, the downstream layers receive the discretized value, while the gradients received are copied over to the continuous logits, allowing for gradient flow. Intuitively, standard Gumbel-Softmax sampling stochastically provides a probability distribution across layers, after which we sample the L -most likely layers via

discretization, and copy the gradients across the discretization step. We provide justification in Appendix A.2.

4. Implementation Details

ADMN Application Domain: To showcase the generality of ADMN, we evaluate it on two highly diverse tasks - regression and classification. We select distributed multimodal localization as the regression task and multimodal human activity recognition for classification. For the task of distributed multimodal localization, we follow the approach in (Jeong et al., 2024). Assuming S sensor nodes each containing M modalities, we define M modality-specific backbones that process each node’s data, resulting in $S \times M$ backbone embeddings. The $S \times M$ embeddings are provided as input tokens into the transformer encoder for fusion, and the output head converts the fused embedding into a prediction of target location. For multimodal human activity recognition, we employ the popular *space-time encoder* architecture (Woo et al., 2023). Given F frames of an activity from M modalities, we define M backbones that process each frame of data, resulting in $F \times M$ embeddings. Once again, a stack of transformer encoders fuses the embeddings, and the output head predicts the activity class. In this work, we restrict the majority of our evaluations to image-like data (e.g., RGB, depth) that can utilize the same set of MAE ImageNet initializations. However, we hope that our work inspires future models to be pretrained with LayerDrop, removing the heavy pretraining burden and allowing the user to proceed directly to Stage 1 Training.

MAE Pretraining: We pretrain Vision Transformers on the ImageNet-1K dataset with the Masked Autoencoders method. Additionally, we employ a LayerDrop probability of 0.2 in each layer of the encoder. We follow the standard pretraining process for a ViT-Base model with 12 layers and dimension 768. We refer to the original paper (He et al., 2022) for further implementation details.

Training Details: To accomplish the goal of adjusting to variable modality QoI, ADMN must understand how to process noisy multimodal input. In addition to employing LayerDrop, we also add varying amounts of noise to the multimodal inputs during Stage 1 Training. We simulate dynamic QoI by adding Gaussian Noise of different standard deviations to each modality, allowing the model to gain robustness to noisy inputs during finetuning. For each modality m_i in a batch of input samples, we will draw $\sigma_{m_i} \sim [0, \sigma_{i_{max}}]$, and then add zero mean Gaussian Noise with standard deviation σ_{m_i} (i.e., $\mathcal{N}(0, \sigma_{m_i})$) to modality m_i . This ensures the controller can properly perform QoI-aware layer allocation during Stage 2 Training. Further details and hyperparameter settings are provided in Appendix A.3.

Table 1. Left: GDTM Localization Error (cm) ↓. Right: MM-Fi Classification Accuracy ↑. Best viewed in color

Noise Type	Layers	Upper Bound	ADMN	Naive Scratch	Naive Alloc.	Image Only	Depth Only
Binary	6		24.9 64.1%	46.6 3.7%	104.0 7.7%	63.3 29.0%	64.8 36.4%
	8	21.1 72.5%	22.5 69.3%	42.6 3.7%	78.2 31.5%	56.9 34.9%	52.8 57.1%
	12		21.8 73.1%	48.2 3.7%	27.4 53.1%	58.1 37.7%	51.5 58.6%
	16		20.8 73.6%	44.5 3.7%	22.1 72.8%	—	—
Discrete	6		51.8 35.0%	39.1 3.7%	112.5 5.6%	67.5 18.8%	85.0 17.6%
	8	29.6 44.4%	37.5 40.5%	36.7 3.7%	97.6 13.0%	53.2 18.5%	61.7 30.9%
	12		32.5 41.5%	40.4 3.7%	46.9 29.0%	53.7 23.1%	58.6 32.7%
	16		30.5 42.4%	37.3 3.7%	31.0 42.9%	—	—
Continuous	6		53.8 31.7%	49.4 3.7%	117.3 4.0%	77.8 8.3%	83.8 17.3%
	8	31.6 45.1%	42.2 39.0%	46.4 3.7%	105.3 11.1%	64.7 19.8%	58.0 34.9%
	12		36.6 40.4%	51.6 3.7%	51.7 20.1%	64.7 18.2%	55.4 35.5%
	16		33.8 43.1%	48.4 3.7%	33.3 42.0%	—	—

5. Evaluations

5.1. Experimental Setup

5.1.1. DATASETS

The GDTM localization dataset (Jeong et al., 2024) contains multimodal data (RGB, depth, mmWave radar, multichannel audio) of a small remote-controlled car driving on an indoor track. The dataset is also *distributed*, containing 3 sensor nodes each with a full set of modalities. We specifically leverage the distributed vision and depth data to localize the car. For human activity recognition, we use the multimodal MM-Fi (Yang et al., 2024) dataset containing 40 subjects with 27 total activities captured by RGB cameras, depth cameras, mmWave radar, and WiFi. We focus on the visual modalities (RGB, depth) for classification. These datasets do not naturally contain varying modality QoI, so we synthetically add Gaussian Noise to each multimodal input and clip the values between 0 and 1 to simulate different QoI. Although we focus specifically on Gaussian Noise due to its simplicity and irreversible nature, we emphasize that ADMN’s design is generalizable and not designed specifically for Gaussian Noise. We define three categories of Gaussian Noise employed during Stage 2 Training: *binary*, *discrete*, and *continuous*.

Binary: Every modality has an 50% likelihood of either suffering extreme noise corruption, or being left unmodified. This is represented by adding either $\mathcal{N}(0, 0)$ or $\mathcal{N}(0, \sigma_{i_{max}})$ Gaussian Noise to a given modality, generating various combinations of noisy and clean modalities. The real-world analog involves flickering sensor feeds alternating between clean and severely degraded transmissions.

Discrete: We extend the binary case to a larger set of standard deviations encompassing noisy, yet still informative data. We add $\mathcal{N}(0, \sigma_{i_j})$ to every modality i ’s input data.

Each modality defines a finite set of N_i standard deviations $\{\sigma_{i_1}, \sigma_{i_2}, \sigma_{i_3}, \dots, \sigma_{i_{N_i}}\}$ from which σ_{i_j} is drawn. This setting is representative of systems deployed in environments with a finite set of conditions (e.g., indoor lighting 25%, 50%, 100%), or even sensors that contain different settings such as ISO levels in cameras.

Continuous: Instead of drawing σ_{i_j} from a finite set, we instead draw σ_{i_j} from a continuous range $[0, \sigma_{i_{max}}]$ defining the allowable range of standard deviations. The continuous case represents highly dynamic noise settings that are difficult to decompose into a finite set of scenarios.

5.1.2. BASELINES

We present the following baselines:

Upper Bound: We do not drop any layers, allocating the full 12 layers to each backbone. This represents the best performance with maximum layer budget.

Naive Allocation: This baseline represents input-agnostic allocation. Given a layer budget L and M modalities, we naively allocate $\frac{L}{M}$ layers to each backbone following every-other allocation.

Image Only: All L layers are allocated to the Image modality, valid only for $L \leq 12$

Depth Only: All L layers are allocated to the Depth modality, valid only for $L \leq 12$.

Naive Scratch: We train a network *from scratch without LayerDrop* on the downstream task with each backbone containing $\frac{L}{M}$ layers. As this model is statically provisioned, we train a new ‘‘Naive Scratch’’ model for every layer budget L . Although impractical due to the high training cost, it nonetheless serves a useful comparison.

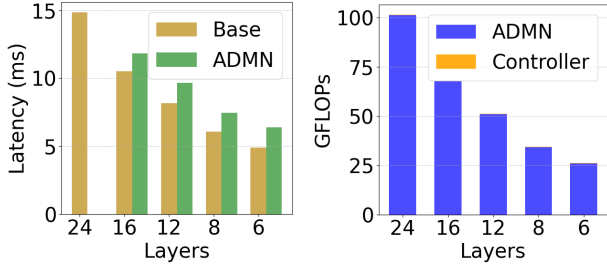


Figure 4. Latency (ms) and GFLOPs vs Layers for GDTM

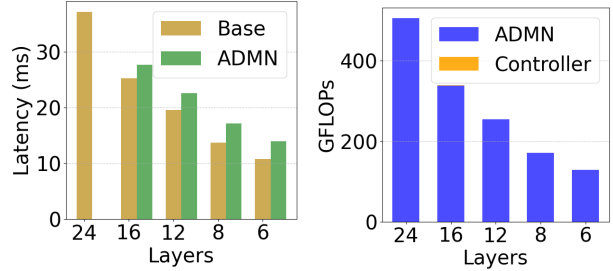


Figure 5. Latency (ms) and GFLOPs vs Layers for MM-Fi

5.1.3. METRICS

For the localization task, we use the average localization error (measured in cm) as the evaluation metric. For the classification task, we evaluate performance using classification accuracy, a standard metric that measures the proportion of correctly predicted labels. In addition, we calculate the FLOPs (Floating Point Operations) of each network to assess computational efficiency, highlighting the trade-off between performance and resource consumption.

5.2. Localization Results

Localization Error: We compare ADMN’s localization error to every baseline tested on the three noise categories in Table 1, shown in **dark green**. We observe the greatest boost in performance in the Binary case, where the model achieves localization performance competitive with the Upper Bound with only 6 layers. This demonstrates that the controller has correctly allocated resources towards high QoI modalities in every sample. In comparison, the high error of the baselines reveals how input-aware layer allocation is invaluable in low-compute settings. The Discrete case, which is an extension of the Binary case with various levels of noise, also benefits from introducing ADMN. The 6 layer allocation incurs higher error, but the error sharply drops as we move to 8 layers. Interestingly, the Naive Scratch baseline outperforms ADMN in the 6 and 8 layer Discrete case, but fails to maintain its advantage at larger layer allocations. We hypothesize that the Naive Scratch models are more competitive at smaller layer budgets as proper initialization with pretrained weights has a greater impact in deeper networks. We observe similar trends in the Continuous case.

Localization Compute: Figure 4 shows the meaningful reductions in floating-point operations and latency when employing ADMN. Although the controller accounts for a significant proportion of the latency at smaller layer budgets ($\sim 20\%$), the high throughput at these latencies (> 150 fps) surpasses most sensor sampling rates. Moreover, ADMN’s controller utilizes a negligible amount of FLOPs. The controller consumes only 0.26 GFLOPs, which constitutes about 1% of the model’s total operations at *the fewest allocation of 6 layers*. When viewing Table 1 in context of these metrics, we can observe the significance of ADMN. In

the Binary case, ADMN localizes within 4 cm of the Upper Bound while reducing latency by $\sim 60\%$ and FLOPs by $\sim 75\%$. With the more complex Discrete case, employing 8 layer allocation incurs 8 cm of additional error, but cuts latency and FLOPs by $\sim 50\%$ and $\sim 65\%$, respectively. Even in the difficult Continuous case, using a 12 layer allocation reduces latency and FLOPs by 35% and 50%, respectively, with only 5 cm of additional error.

5.3. Classification Results

Classification Accuracy: ADMN’s classification accuracy on the MM-Fi dataset is shown in **dark blue** in Table 1. Similarly to its localization performance, ADMN exhibits significant gains in the Binary noise case over the baselines, outperforming the second best Depth-only baseline by 28% with a 6 layer budget. We observe similar trends in the Discrete and Continuous cases. Notably, one key difference in classification is the poor performance of the Naive Scratch model. Regardless of the number of layers, training the model purely from scratch did not converge, highlighting the importance of prior weight initialization. With ADMN, one can initialize a full-size model with pretrained weights, enabling easier convergence, and then simply trim the model size by disabling layers.

Classification Compute: We observe in Figure 5 that the total GFLOPs are once again dominated by the main network, with the controller accounting for only 0.2% of the total GFLOPs at the smallest configuration of 6 layers, and 0.07% with 16 layers. The controller constitutes a larger proportion of total latency, but the accuracy gain of QoI-aware allocation far outweighs the small latency increase.

5.4. Additional Modalities

To ensure that ADMN can generalize beyond two vision-based modalities, we incorporate mmWave radar and perform localization on GDTM with RGB, depth, and mmWave modalities. Figure 6 shows a CDF of the error when tested on the 12-Layer Binary case, demonstrating that ADMN retains good performance with three modalities that contain significant heterogeneity.

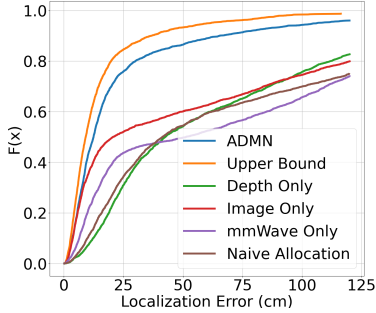


Figure 6. Localization Error CDF with Three Modalities

5.5. Dynamic Compute Constraints

One drawback is that the ADMN controller is trained only for one particular layer budget L . Consequently, we must employ multiple controllers to adapt to *dynamic test-time compute requirements* induced by factors such as thermal throttling. Nevertheless, the training overhead for the controllers is low (Appendix A.1), enabling a controller to be trained for every layer budget. As the main network is frozen during controller training, all the controllers are compatible with the same set of main network weights. Additionally, the controller constitutes only 2.3% and 3.2% of the total network parameters in the localization and classification tasks, respectively, allowing for easy storage on disk. As a result, ADMN is highly capable of tackling fluctuating compute requirements. Imagine a scenario where due to thermal throttling, 25% of execution time lies in the 6 layer regime while the rest allows for 16 layers. Assuming that the system must function at all times, a statically provisioned model has two choices - use a six layer model at all times, or separately train and store a 6 layer model and 16 layer model. The first scenario sacrifices accuracy, while the second scenario not only requires significant investment in training time, but also must store two separate, large models in memory.

5.6. Ablation Study

Efficacy of LayerDrop: LayerDrop is integrated into two stages - initial MAE pretraining on ImageNet, and subsequent finetuning on the desired task. Figure 7 showcases the localization error on the GDTM dataset as the number of dropped layers increases in separate unimodal depth and image networks. We observe that adding LayerDrop during finetuning has the greatest impact, but benefit is observed in both cases, allowing us to drop a meaningful amount of layers with negligible degradation. These results confirm that LayerDrop is compatible with the ViT architecture, MAE pretraining, and is also effective when finetuned on another task. We present additional results in Appendix A.4.

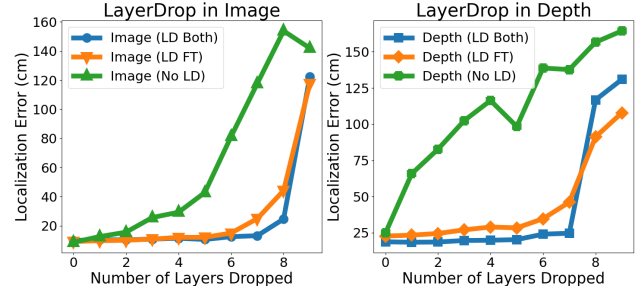


Figure 7. Effect of LayerDrop on 12-layer unimodal image and depth localization networks. “No LD” indicates no use of LayerDrop, “LD FT” indicates use only during finetuning, and finally “LD Both” employs LayerDrop in both phases

6. Discussion

Batched Inference: In ADMN, the layer allocation is decided by the controller prior to backbone execution, enabling support for batched inference. Classically, adaptive models cannot support batched inference as different samples will proceed through different layers. However, since ADMN decides the layer allocation at the controller, we can group samples into *sub-batches* based on similar layer allocation. For instance, samples with high depth noise and low image noise will activate a similar set of layers, allowing them to be grouped together for batched execution.

Fusion with Early Exit: While ADMN and unimodal Early-Exit methods tackle fundamentally different problems, the two techniques can be combined for further computation efficiency. ADMN’s controller always allocates L layers across all the modalities. However, on simple inputs, all L layers may not be necessary, allowing for Early-Exit techniques to be integrated for further performance gains.

7. Conclusion

This paper proposes ADMN, a multimodal network capable of dynamically adjusting the number of active Transformer layers across modalities according to the quality of each sample’s input modalities. Through this continuous reallocation, ADMN can match the accuracy of far larger networks while utilizing a fraction of their operations. Additionally, the dynamic backbones of ADMN are also well suited for scenarios with adaptive compute, ranging from heterogeneous deployment devices to fluctuating energy availability. We demonstrate the superiority of ADMN compared to other baselines across both classification and localization tasks.

Impact Statement

This paper presents work whose goal is to advance the field of Machine Learning. There are many potential societal consequences of our work, none which we feel must be specifically highlighted here.

Acknowledgments

The research reported in this paper was sponsored in part by the DEVCOM Army Research Laboratory (award # W911NF1720196), the Air Force Office of Scientific Research (awards # FA95502210193 and FA95502310559), and the National Institutes of Health (award # 1P41EB028242). The views and conclusions contained in this document are those of the authors and should not be interpreted as representing the official policies, either expressed or implied, of the funding agencies. Jason Wu was supported by the Department of Defense (DoD) through the National Defense Science & Engineering Graduate (NDSEG) Fellowship Program.

References

- Bengio, Y., Léonard, N., and Courville, A. Estimating or propagating gradients through stochastic neurons for conditional computation. *arXiv preprint arXiv:1308.3432*, 2013.
- Cai, Q., Liu, X., Zhang, K., Xie, X., Tong, X., and Li, K. Acf: An adaptive compression framework for multimodal network in embedded devices. *IEEE Transactions on Mobile Computing*, 23(5):5195–5211, 2024. doi: 10.1109/TMC.2023.3303350.
- Chen, Y.-T., Shi, J., Ye, Z., Mertz, C., Ramanan, D., and Kong, S. Multimodal object detection via probabilistic ensembling. In *European Conference on Computer Vision*, pp. 139–158. Springer, 2022.
- Dosovitskiy, A. An image is worth 16x16 words: Transformers for image recognition at scale. *arXiv preprint arXiv:2010.11929*, 2020.
- Eitel, A., Springenberg, J. T., Spinello, L., Riedmiller, M., and Burgard, W. Multimodal deep learning for robust rgb-d object recognition. In *2015 IEEE/RSJ International Conference on Intelligent Robots and Systems (IROS)*, pp. 681–687, 2015. doi: 10.1109/IROS.2015.7353446.
- Fan, A., Grave, E., and Joulin, A. Reducing transformer depth on demand with structured dropout. *arXiv preprint arXiv:1909.11556*, 2019.
- Gao, R., Oh, T.-H., Grauman, K., and Torresani, L. Listen to look: Action recognition by previewing audio. In *Proceedings of the IEEE/CVF conference on computer vision and pattern recognition*, pp. 10457–10467, 2020.
- He, K., Chen, X., Xie, S., Li, Y., Dollár, P., and Girshick, R. Masked autoencoders are scalable vision learners. In *Proceedings of the IEEE/CVF conference on computer vision and pattern recognition*, pp. 16000–16009, 2022.
- Jeong, H. L., Wang, Z., Samplawski, C., Wu, J., Fang, S., Kaplan, L. M., Ganesan, D., Marlin, B., and Srivastava, M. Gdtm: An indoor geospatial tracking dataset with distributed multimodal sensors. *arXiv preprint arXiv:2402.14136*, 2024.
- Kim, W., Son, B., and Kim, I. Vilt: Vision-and-language transformer without convolution or region supervision. In *International conference on machine learning*, pp. 5583–5594. PMLR, 2021.
- Lin, R. and Hu, H. Missmodal: Increasing robustness to missing modality in multimodal sentiment analysis. *Transactions of the Association for Computational Linguistics*, 11:1686–1702, 2023.
- Liu, W., Qiu, J.-L., Zheng, W.-L., and Lu, B.-L. Comparing recognition performance and robustness of multimodal deep learning models for multimodal emotion recognition. *IEEE Transactions on Cognitive and Developmental Systems*, 14(2):715–729, 2022. doi: 10.1109/TCDS.2021.3071170.
- Maddison, C. J., Mnih, A., and Teh, Y. W. The concrete distribution: A continuous relaxation of discrete random variables. *arXiv preprint arXiv:1611.00712*, 2016.
- Manzoor, M. A., Albarri, S., Xian, Z., Meng, Z., Nakov, P., and Liang, S. Multimodality representation learning: A survey on evolution, pretraining and its applications. *ACM Trans. Multimedia Comput. Commun. Appl.*, 20(3), October 2023. ISSN 1551-6857. doi: 10.1145/3617833. URL <https://doi.org/10.1145/3617833>.
- Meng, L., Li, H., Chen, B.-C., Lan, S., Wu, Z., Jiang, Y.-G., and Lim, S.-N. Adavit: Adaptive vision transformers for efficient image recognition. In *Proceedings of the IEEE/CVF Conference on Computer Vision and Pattern Recognition*, pp. 12309–12318, 2022.
- Mullapudi, R. T., Mark, W. R., Shazeer, N., and Fatahalian, K. Hydranets: Specialized dynamic architectures for efficient inference. In *Proceedings of the IEEE Conference on Computer Vision and Pattern Recognition*, pp. 8080–8089, 2018.
- Panda, R., Chen, C.-F. R., Fan, Q., Sun, X., Saenko, K., Oliva, A., and Feris, R. Adamml: Adaptive multi-modal learning for efficient video recognition. In *Proceedings of the IEEE/CVF international conference on computer vision*, pp. 7576–7585, 2021.
- Russakovsky, O., Deng, J., Su, H., Krause, J., Satheesh, S., Ma, S., Huang, Z., Karpathy, A., Khosla, A., Bernstein, M., Berg, A. C., and Fei-Fei, L. ImageNet Large Scale Visual Recognition Challenge. *International Journal of Computer Vision (IJCV)*, 115(3):211–252, 2015. doi: 10.1007/s11263-015-0816-y.

- Samplawski, C., Fang, S., Wang, Z., Ganesan, D., Srivastava, M., and Marlin, B. M. Heteroskedastic geospatial tracking with distributed camera networks. In Evans, R. J. and Shpitser, I. (eds.), *Proceedings of the Thirty-Ninth Conference on Uncertainty in Artificial Intelligence*, volume 216 of *Proceedings of Machine Learning Research*, pp. 1805–1814. PMLR, 31 Jul–04 Aug 2023. URL <https://proceedings.mlr.press/v216/samplawski23a.html>.
- Wang, M., Xing, J., Jiang, B., Chen, J., Mei, J., Zuo, X., Dai, G., Wang, J., and Liu, Y. A multimodal, multi-task adapting framework for video action recognition. In *Proceedings of the AAAI Conference on Artificial Intelligence*, volume 38, pp. 5517–5525, 2024.
- Woo, S., Lee, S., Park, Y., Nugroho, M. A., and Kim, C. Towards good practices for missing modality robust action recognition. In *Proceedings of the AAAI Conference on Artificial Intelligence*, volume 37, pp. 2776–2784, 2023.
- Xie, S. M. and Ermon, S. Reparameterizable subset sampling via continuous relaxations. *arXiv preprint arXiv:1901.10517*, 2019.
- Xin, J., Tang, R., Lee, J., Yu, Y., and Lin, J. DeeBERT: Dynamic early exiting for accelerating BERT inference. *arXiv preprint arXiv:2004.12993*, 2020.
- Xue, Z. and Marculescu, R. Dynamic multimodal fusion. In *Proceedings of the IEEE/CVF Conference on Computer Vision and Pattern Recognition*, pp. 2575–2584, 2023.
- Yang, J., Huang, H., Zhou, Y., Chen, X., Xu, Y., Yuan, S., Zou, H., Lu, C. X., and Xie, L. Mm-fi: Multi-modal non-intrusive 4d human dataset for versatile wireless sensing. *Advances in Neural Information Processing Systems*, 36, 2024.
- Yin, J., Shen, J., Chen, R., Li, W., Yang, R., Frossard, P., and Wang, W. Is-fusion: Instance-scene collaborative fusion for multimodal 3d object detection. In *Proceedings of the IEEE/CVF Conference on Computer Vision and Pattern Recognition*, pp. 14905–14915, 2024.
- Zhou, W., Xu, C., Ge, T., McAuley, J., Xu, K., and Wei, F. BERT Loses Patience: Fast and Robust Inference with Early Exit. In *Advances in Neural Information Processing Systems*, volume 33, pp. 18330–18341, 2020.

A. Appendix

A.1. Controller Training Overhead

We found it sufficient to train the controller for 10 and 15 epochs on the localization and classification tasks, respectively. We attribute this to the simple end-to-end training recipe in which we avoid complex reinforcement learning. On a Nvidia RTX 4090, training the localization controller took only 27 min.

Noise Type	Seed	6 Layers	8 Layers	12 Layers	16 Layers
Binary	100	25.62	22.40	21.37	20.87
	200	24.49	22.56	21.88	20.66
	300	24.60	22.56	22.10	20.75
Discrete	100	51.96	36.35	32.24	29.38
	200	47.29	39.12	33.01	30.95
	300	56.09	37.02	32.11	31.27
Continuous	100	54.47	42.92	36.18	32.55
	200	53.25	42.20	36.96	33.66
	300	53.59	41.56	36.73	35.25

Table 2. ADMN Localization Error (cm) ↓. Shown previously in Table 1 with averaging

Task	Seed	6 Layers	8 Layers	12 Layers	16 Layers
Finite	100	73.60	64.32	56.15	21.54
	200	98.77	49.90	24.30	22.17
	300	62.36	63.68	23.23	21.90
Discrete	100	118.14	90.36	73.87	32.15
	200	94.43	58.66	50.76	51.32
	300	103.21	82.20	51.84	29.81
Continuous	100	87.90	55.42	75.52	36.51
	200	96.32	118.54	42.46	31.16
	300	78.65	86.94	78.57	34.23

Table 3. Straight-Through Estimator Localization Error (cm) ↓

A.2. Justification of Gradient Propagation Technique in the Controller

Directly Employing the Straight-Through Estimator: ADMN utilizes the combination of standard temperature Gumbel-Softmax sampling and the straight-through estimator to propagate gradients over the discretization to the continuous logits. One natural question is whether Gumbel-Softmax Sampling is necessary, as one could theoretically apply discretization on the raw logits and propagate gradients with the straight-through estimator. In Table 2 and Table 3, we present the localization results on the GTDM dataset across different layer configurations and noise categories, with three seeds for each experiment. The results highlight that Gumbel-Softmax sampling plays an important role in model training.

This behavior can be attributed to several reasons. First, by applying the softmax function to the logits, we convert them into probability values where one logit’s high probabilities come at the expense of the others. As a result, the softmax function encourages the controller to select only the L best performing layers for some value of noise and minimize the probability of the remaining layers. Additionally, utilizing the Gumbel distribution also introduces *stochasticity* into the sampling process. Instead of always selecting the top- L logits as the active layers, the stochasticity intuitively serves to encourage *exploration* of different layer configurations.

Progressive Top- L Gumbel Softmax Sampling: Instead of employing the straight-through estimator, one can also utilize repeated Gumbel-Softmax Sampling to emulate discrete top- L sampling. (Xie & Ermon, 2019) proposed a method to emulate discrete top- L sampling by repeatedly applying the softmax function L times while adjusting the logits each

iteration. However, these methods may cause issues when applied to ADMN. First, methods utilizing Gumbel-Softmax Sampling to emulate discrete distributions typically have to undergo *temperature annealing* (Maddison et al., 2016), where the temperature is slowly decreased until the distribution is approximately categorical. Utilizing annealing can lead to a longer and more complicated training process for the controller. Additionally, the lack of explicit discretization during training may also result in a distribution shift at inference time, where the controller may learn to overrely upon partially activated layers during training.

A.3. Training Details:

Parameter	Value
Epochs	400
Learning Rate	1E-4
Scheduler	LinearLR
Optimizer	Adam
LayerDrop	0.2
Fusion Layers	6
Fusion Dimension	64
Fusion Heads	4
Modality Dropout	0.1
Depth Noise	[0, 3]
Image Noise	[0, 2]

Table 4. MM-Fi Finetuning

Parameter	Value
Epochs	400
Learning Rate	5.00E-04
Optimizer	Adam
LayerDrop	0.2
Fusion Layers	6
Fusion Dimension	256
Fusion Heads	4
Modality Dropout	0.1
Depth Noise	[0, 0.75]
Image Noise	[0, 3]

Table 5. GDTM Finetuning

Parameter	Value
Epochs	10/15
Learning Rate	1.00E-03
Scheduler	LinearLR
Gumbel Temperature	1

Table 6. Controller Training

MM-Fi Classification: We depict the Stage 1 details for the MMFI Classification main network in Table 4. We employ the same 12 Layer ViT-Base model from pretraining. After we obtain the embeddings from the backbones, they are fused through a stack of Transformer Encoders with the details shown above. We employ a 0.2 LayerDrop rate and add Gaussian Noise with a randomly drawn standard deviation to the input for every batch. The image Gaussian Noise standard deviation is uniformly drawn from the range 0 to 2 and the depth noise is drawn from the range 0 to 3.

GDTM Localization: The training details are shown in Table 5. Similarly to the MM-Fi Classification Model, we use a Transformer Encoder to perform multimodal fusion. The range of standard deviations for depth is smaller due to increased sensitivity of the depth modality in this dataset.

A.4. Additional LayerDrop Results

Removed Layer Indices	Normal Pre + Normal FT	LayerDrop Pre + Normal FT	Normal Pre + LayerDrop FT	LayerDrop Pre + LayerDrop FT
None	81.16%	80.36%	79.91%	78.92%
6	79.99%	79.35%	79.61%	78.59%
6, 8	77.20%	76.77%	78.68%	77.72%
4, 6, 8	72.97%	73.94%	77.64%	76.84%
2, 4, 6, 8	70.01%	71.48%	76.90%	76.37%
2, 4, 6, 8, 10	64.27%	65.07%	75.44%	74.70%
2, 4, 6, 7, 8, 10	33.91%	38.76%	69.83%	69.28%
1, 2, 4, 6, 7, 8, 10	13.74%	23.60%	66.67%	66.94%

Table 7. ImageNet-1K performance with different layer indices removed. Normal refers to a LayerDrop rate of 0, while LayerDrop refers to utilizing a LayerDrop rate of 0.2. Pre indicates the MAE pretraining stage, while FT refers to supervised finetuning on ImageNet-1K.

The ViT models are first pretrained on the ImageNet dataset with Masked Autoencoder pretraining, in which we add LayerDrop. To understand its performance on the ImageNet-1K dataset, we perform a subsequent stage of supervised learning on the ImageNet dataset to obtain the validation accuracy. Table 7 reveals the validation accuracy on the ImageNet-1K dataset with various dropped layers, and with LayerDrop integrated into different stages of training. When comparing the

model trained without any usage of LayerDrop to the one in which LayerDrop was employed in both stages, we can observe an accuracy improvement of over 50% when 7 layers are dropped during inference time. Curiously, given that LayerDrop is added during supervised finetuning, applying MAE pretraining with LayerDrop does not appear to be necessary in ImageNet-1K. However, the results in Figure 7 showcase that it has an impact on downstream tasks.

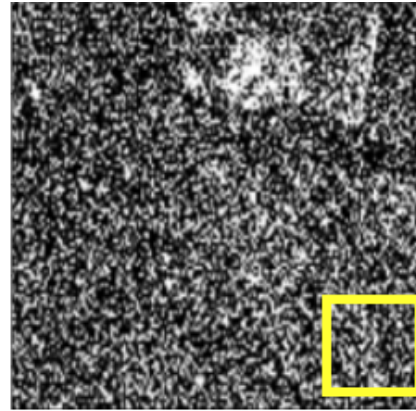
A.5. Qualitative Results

In Figure 8, we visually showcase the noise corrupted multimodal inputs, and the corresponding layer allocation output by the ADMN controller with a budget of 6 layers. Given that the depth modality is naturally lower QoI, we can see that the controller gives preference towards the image modality. When Image Noise Standard Deviation is 3 and Depth Noise Standard Deviation is 0.25, the controller equally allocates layers among the two modalities. However, when the depth is entirely clean, the controller recognizes this and allocates all the layers towards the clean depth modality. These results reveal the intelligent allocation of the ADMN controller. For stability reasons, the first layer of the backbone is always activated.



Image Noise Standard Deviation: **0**

Selected Layers:
[1 0 0 0 1 0 1 0 1 0 0 1]



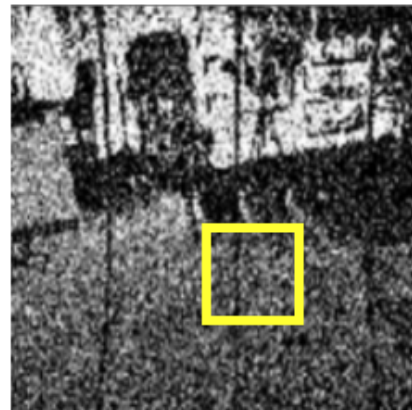
Depth Noise Standard Deviation: **0.75**

Selected Layers:
[1 0 0 0 0 0 0 0 0 0 0 0]



Image Noise Standard Deviation: **1**

Selected Layers:
[1 0 0 0 1 1 1 0 0 0 0 1]



Depth Noise Standard Deviation: **0.25**

Selected Layers:
[1 0 0 0 0 0 0 0 0 0 0 0]

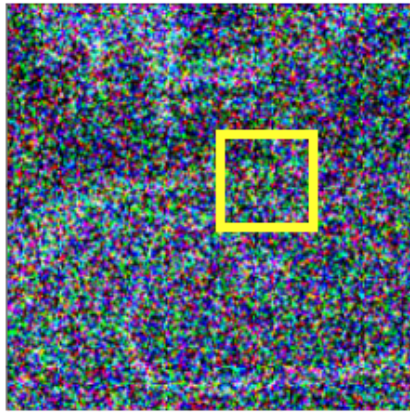
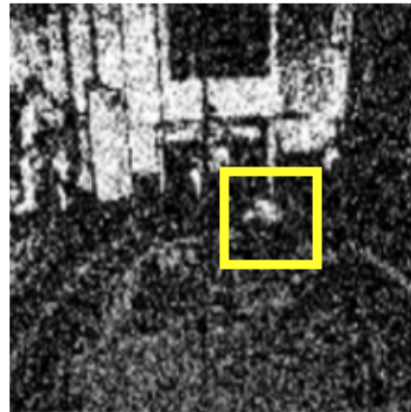


Image Noise Standard Deviation: **3**

Selected Layers:
[1 0 0 0 0 1 0 0 0 0 0 1]



Depth Noise Standard Deviation: **0.25**

Selected Layers:
[1 0 0 0 0 0 1 1 0 0 0 0]

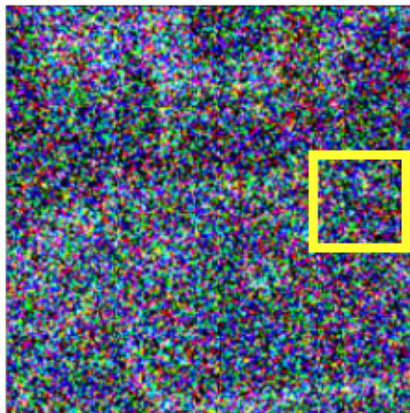
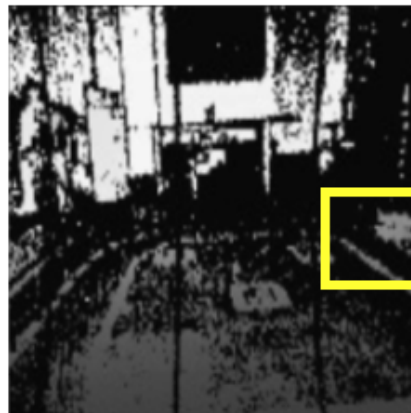


Image Noise Standard Deviation: **3**

Selected Layers:
[1 0 0 0 0 0 0 0 0 0 0 0]



Depth Noise Standard Deviation: **0**

Selected Layers:
[1 0 0 0 1 0 0 0 1 0 1 1]

Figure 8. Visual Results on the GDTM Dataset highlighting the impact of noise and featuring the controller layer allocation